Summary of Propulsive-Lift Research in the Langley 16-Ft Transonic Tunnel

Francis J. Capone*
NASA Langley Research Center, Hampton, Va.

A summary of research on both conceptual and practical configurations in which the aircraft's powerplant is integrated to take advantage of propulsion-induced aerodynamics conducted in the Langley 16-foot transonic has been made. These investigations included: 1) vectoring a partial-span jet exhaust at a wing trailing edge; 2) thrust vectoring characteristics of a twin, two-dimensional variable-geometry wedge nozzle; and 3) a jet exhaust/upper surface blowing concept for fighter aircraft. These studies indicate a potential for increasing maneuverability of fighter aircraft at high lift coefficients. With proper integration of the powerplant into the airframe, significant improvements in cruise performance of both fighter and transport aircraft are possible.

Nomenclature†

C_D	= drag coefficient
C_L	= lift coefficient
$C_{L,0}$	= jet-off lift coefficient
$C_{L,j}$	= measured jet lift coefficient, $C_T \sin(\alpha+\delta)$
$C_{L,\Gamma}$	= jet-induced supercirculation lift coefficient
ΔC_L	= incremental lift coefficient, $C_L - C_{L,0}$
C_T	= gross-thrust coefficient
$C_{T,i}$	= ideal thrust coefficient
F_i	= ideal thrust
F_j	= thrust along nozzle axis
$(F-D)/F_i$	= thrust-minus-drag performance parameter
$\Delta F/F_i$	= nondimensional thrust increment
G	= gain factor
M	= freestream Mach number
$p_{t,j}/p_\infty$	= nozzle pressure ratio
α	= angle of attack, deg
δ	= measured effective jet turning angle, deg
δ_c	= canard deflection angle, deg
δ_d	= design nozzle deflection angle, deg
δ_F	= Coanda flap angle, deg
δ_h	= horizontal tail deflection, deg
δ_{LE}	= wing leading-edge flap deflection, deg
δ_{static}	= measured static turning angle, deg
δ_{TE}	= wing trailing-edge flap deflection, deg
δ_w	= wedge angle, deg

Introduction

FOR the past 16 years, the staff of the Langley 16-ft transonic tunnel has been actively conducting research on a variety of both conceptual and flying aircraft employing vectored or reverse thrust. An investigation was made in 1959 on the variable-sweep all-wing "Swallow."[1,2] Control of this airplane would have been accomplished by vectoring outboard turbojet engine nacelles located above and below the wings in both the pitch and yaw planes. In 1960, the V/STOL Hawker P.1127 airplane model[3,4] was tested in order to determine jet interference effects with the nozzles in the cruise mode.

The Adam-II concept, tested in 1967, featured a propulsive wing[5] in which large tip-turbine driven fans were located along the wing span. Vectoring V/STOL performance was accomplished by deflecting a large wing trailing-edge flap into the jet exhaust. Two investigations have been concerned with in-flight thrust reversing. These included tests conducted in 1969 with the F-11-F airplane[6,7] and a Gulfstream-II aircraft configured for use as an in-flight simulator for training pilots for the space shuttle.

This paper will summarize recent research on both conceptual and practical configurations in which the aircraft's powerplant is integrated to take advantage of the potential benefits of propulsion induced aerodynamics in order to improve not only cruise efficiency, but also maneuvering performance. These include:

1) vectoring a partial-span jet exhaust at a wing trailing edge; 2) thrust vectoring characteristics of a twin, two-dimensional, variable-geometry wedge nozzle; and 3) an upper surface blowing concept for fighter aircraft.

These investigations have all been conducted in the Langley 16-ft transonic tunnel at Mach numbers up to 0.95 and over a Reynolds number per meter range of 8.20×10^6 to 13.12×10^6. All models were strut-sting supported in the wind tunnel, and all tests were conducted with boundary-layer transition strips fixed.

Vectored Thrust Concept

The Langley Research Center has proposed to integrate a vectorable rectangular exhaust nozzle in an aircraft's fuselage at the wing trailing edge.[8] The effect of the vectored exhaust is to induce lift on the wings due to supercirculation similar to that of a jet flap. In contrast to the jet flap, however, this concept permits the use of all the engine exhaust to simulate a partial-span, thick jet flap; avoids ducting through the wings; and limits mechanical articulation to only the exhaust nozzles. This system has the potential for increasing both maneuverability and cruise performance.

The results of exploratory studies[8,9] are summarized in Fig. 1. The left side shows incremental lift characteristics where the jet-off lift has been subtracted from the total lift measured with the jet operating. Incremental lift is simply defined as

$$\Delta C_L = C_L - C_{L,0} \tag{1}$$

Jet lift is also shown in Fig. 1 for reference. This model had only one force balance, and therefore, jet lift is computed at forward speeds using the measured static turning angle. For a nozzle with 30° deflection at $M=0.7$ and $\alpha=0$, the jet induced supercirculation lift $C_{L,\Gamma}$ was about twice that of the jet lift where induced lift is the difference between incremental and jet lift.

Thrust recovery as a function of Mach number for $\delta_d=30°$ is shown on the right side of Fig. 1. Thrust recovery, which is defined as that portion of the thrust recovered in the stream-

Presented as Paper 75-1315 at the AIAA/SAE 11th Propulsion Conference, Anaheim, Cal., Sept. 29-Oct. 1, 1975; submitted Sept. 24, 1975; revision received Dec. 31, 1975.

Index categories: Aircraft Aerodynamics (including Component Aerodynamics); Aircraft Configuration Design; Aircraft Powerplant Design and Installation.

*Aerospace Engineer, High-Speed Aerodynamics Division. Member AIAA.

†All forces are nondimensionalized with respect to wing reference area and freestream dynamic pressure.

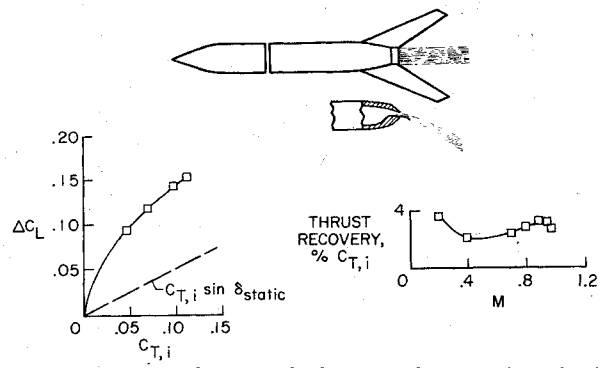

Fig. 1 Summary of vectored thrust exploratory investigation, $\delta_d = 30°$, $M = 0.7$, $\alpha = 0°$.

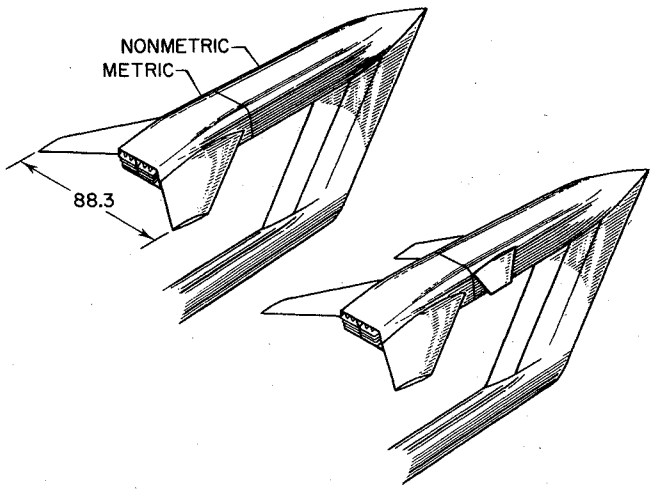

Fig. 2 Sketch of model with and without canard.

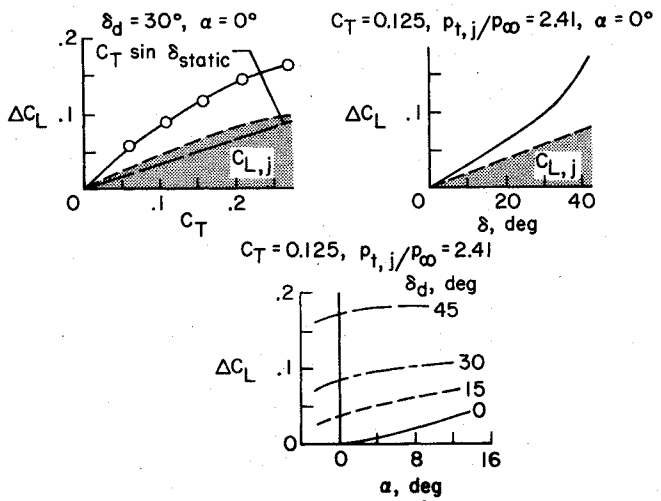

Fig. 3 Effect of varying nozzle deflection angle on incremental lift, $M = 0.7$.

wise direction, was approximately 3% of the ideal thrust. These results of Fig. 1 demonstrated that thrust vectoring can induce lift due to supercirculation, and that thrust recovery was achieved for a three-dimensional configuration at transonic speeds.

The highly swept wing of the configuration shown in Fig. 1 was chosen for two reasons. First, the aerodynamic center could be placed at the nozzle exit in order to minimize the pitching-moment changes due to thrust vectoring. Second, improved lift augmentation was anticipated with the outboard panels of the highly swept wing placed in a stronger induced upwash field created by the deflected jet. It was reasoned that placing the wings in this position would tend to compensate for the short span of the jet. However, the results of Ref. 8 indicated that most of the induced lift was developed on the inboard portion of the wing panels in front of the nozzle exit.

Consequently, another model was designed; one that had a wing planform and airfoil thickness ratio typical of current high-performance twin-engine fighter aircraft. The model shown in Fig. 2 had a twin-jet propulsion simulation system with a twin-bellows arrangement for eliminating transfer of axial momentum across the dual force balance system. The metric system consisted of a double balance "piggyback" arrangement in which one six-component balance measured the total thrust-minus-drag forces on the entire model aft of the metric break, and a second six-component balance measured the internal normal and axial forces on the nozzles. This arrangement allowed for direct measurement of the effective jet turning angle and jet lift at all conditions. Complete model details can be found in Refs. 10 and 11.

The purpose of this investigation was to provide, through a series of parametric studies, the information necessary to properly evaluate the potential of this propulsive-lift concept for use on highly maneuverable aircraft. This study[12] included the effect of nozzle deflection angle, nozzle exit location, nozzle shape and airfoil camber on lift, drag, pitch, and load distributions.

Typical results showing the effects of deflecting a jet at the wing trailing edge are presented in Fig. 3. To the upper left is shown the variation of incremental lift, ΔC_L, with nozzle thrust coefficient for the nozzle with 30° deflection. The nozzle pressure ratio ranged from about 1.9 to 4.6 for these thrust coefficients. The shaded portion of this figure shows measured jet lift to be nonlinear with increasing thrust coefficient. For this nozzle deflection angle, the effective jet turning angle measured by the second force balance decreases with increasing thrust coefficient.[10] However, the effective jet turning angle was always greater than the measured static turning angle. The decrease in effective jet turning with increasing thrust coefficient is believed to be associated with the jet flow separating over the top turning vane of the nozzle. These nozzles had three circular arc turning vanes and depended upon Coanda turning over the top vane for maximum turning. Also presented is a computed jet lift, $C_T \sin \delta_{static}$, based on maximum static turning.

The variation of incremental lift with measured turning angle δ is shown in the upper right portion of Fig. 3. Data are presented at $M = 0.7$, $\alpha = 0°$, and at $C_T = 0.125$. This thrust coefficient corresponds to a typical jet pressure ratio for $M = 0.7$. Lift increment varies linearly with measured turning angle up to 27°.

The effects of angle of attack on lift increment can be seen by examining the lower half of Fig. 3. For the 0° and 15° nozzles, the increase in incremental lift is due to an increase in both jet lift and jet-induced lift. For example, half of the incremental lift for the 0° nozzle at $\alpha = 13.5°$ is induced lift and results from an improved span load distribution from the body to about 0.4 semispan.[10] For the 30° and 45° nozzles, increases in incremental lift are due primarily to an increase in jet lift with increasing angle of attack. In general, angle-of-attack effects on induced lift are small for these two deflection angles.

Thrust recovery characteristics[10,12] for this configuration are shown in Fig. 4 where recovery in terms of percent thrust coefficient is shown as a function of the total lift coefficient C_L. These results are shown for $M = 0.7$ and $C_T = 0.125$. The point at which the curve crosses the zero percent thrust recovery line is at the lift coefficient where the drag polars are no longer parabolic. Increasing nozzle deflection angle not only increases thrust recovery, but also the lift coefficient at which recovery equals zero percent.

Since thrust recovery determined from thrust-minus-drag measurements is approximately equal to recovery determined from drag measurements,[10] increases in recovery are due

primarily to a decrease in drag coefficient. This decrease in drag is due mainly to the induced upwash field created in front of the wing by the deflected jet. Consequently, at a constant angle of attack, the increase in the resultant force vector on the wing is only in the lift direction when there is no increase in drag. Reductions in drag due-to-lift were found for various combinations of nozzle deflection angle and Mach number.[10] In addition, for this configuration, jet operation at vectoring conditions greatly reduces afterbody flow separation at $M=0.90$ and 0.95, which accounts for some further decreases in drag coefficient.

The results of Ref. 12 have been extended to include the effects of a canard on the induced lift characteristics of the wing. The close-coupled canard shown in Fig. 2 was mounted on the nonmetric portion of the model (part of model not mounted on a force balance) above the wing.

A comparison of the lift characteristics for the model with and without canards is shown in Fig. 5. For this comparison, gain factor is used instead of incremental lift where gain factor is defined as

$$G=\frac{\Delta C_L}{C_T \sin \delta_{\text{static}}} \tag{2}$$

The quantity $C_T \sin \delta_{\text{static}}$ is jet lift based on the static turning angle, and is used because the canard tests were conducted without the thrust balance. As can be seen, there is only a small decrease in gain factor over the Mach number range for $\delta_c=0°$, $\alpha=0°$, and $\delta_d=30°$. There can be either small increases or decreases in gain factor, similar to that noted in Fig. 5 for other combinations of the test parameters (M, α, C_T) with the canard at 0° and ±5° deflection.

The variation of incremental lift with angle of attack is shown in Fig. 6 for the model with the canard off and at $\delta_c=-5°$ for $M=0.4$. These results for an uncambered airfoil should be similar for the configuration with the 64A406 airfoil, since airfoil camber effects on induced lift are small for this wing-body model at this Mach number.[12] Again, jet lift is based on static turning angle. The effect of the canard is generally small, as previously indicated. However, note that the induced lift is nearly constant with angle-of-attack variation.

Two-Dimensional Wedge Nozzle

Multimission military aircraft are usually required to operate at subsonic to supersonic speeds over a wide range of engine pressure ratio. The attainment of high performance is very dependent upon the minimization of interference effects resulting from integration of the propulsion system into the airframe. Past aircraft have been built with axisymmetric round nozzles because of their high internal performance and ease of fabrication. However, installation of twin engines with axisymmetric nozzles can result in substantial aft-end drag.[13]

Two-dimensional, variable-geometry wedge nozzles properly integrated into the airframe can reduce this aft-end drag at transonic and supersonic Mach number. The Langley Research Center is currently evaluating this type of nozzle using both a single-engine powered model[14] (collapsing wedge, translating shroud nozzle) and a twin-engine model shown in Fig. 7 (collapsing wedge, fixed shroud nozzles). The two-dimensional wedge nozzle offers additional advantages in that it can be adapted for thrust vectoring or reversing as shown in Fig. 8. This paper will present only vectoring characteristics. Thrust-minus-drag and reversing performance can be found in Ref. 15.

The nozzle configurations shown in Figs. 7 and 8 were tested with the same propulsion simulation system previously described,[10] but using only the thrust-minus-drag balance. Vectoring performance for deflection angles of 12° and 24° was determined by utilizing nozzles with a cambered wedge (wedge has double actuation). Tests were conducted with

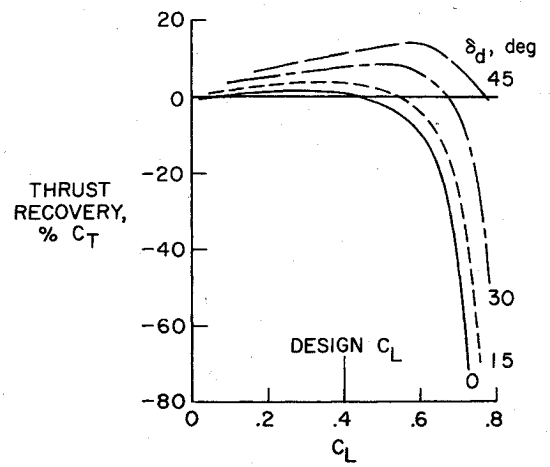

Fig. 4 Effect of varying nozzle deflection angle on thrust recovery, $M=0.7$, $C_T=0.125$, $p_{t,j}/p_\infty=2.41$.

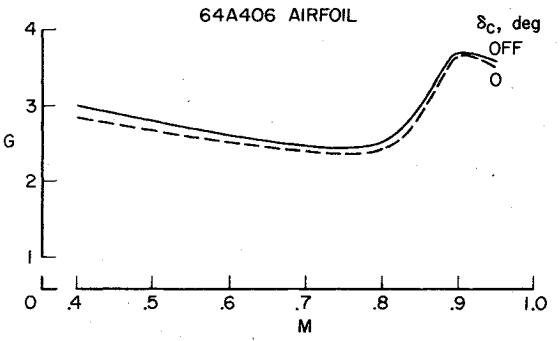

Fig. 5 Effect on nonmetric canard on gain factor, $\delta_d=30°$, $\alpha=0°$, $C_T=0.10$.

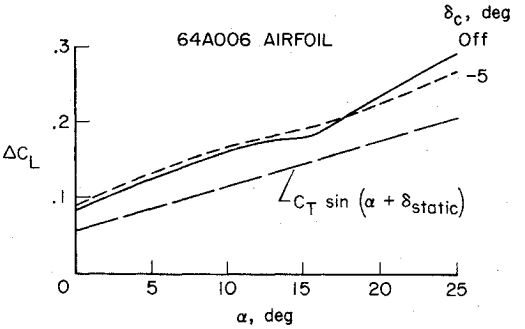

Fig. 6 Effect of nonmetric canard on incremental lift at high angles of attack, $\delta_d=15°$, $M=0.4$, $C_T=0.35$, $p_{t,j}/p_\infty=2.44$.

various combinations of horizontal tails, single and twin vertical tails, and tails off with the nozzle in a nonafterburning mode.

Static turning angle characteristics for the nozzle with wedge angles of 12° and 24° are presented in Fig. 9. Turning angle increases as nozzle pressure ratio is increased to about 4.0, which was the design pressure ratio. The decrease in δ_{static} at pressure ratios greater than 4.0 is probably due to separation over the aft portion of the wedge with separation most likely occurring at the second hinge line location. This results in a loss of the measured nozzle normal force with no effect to the nozzle axial force along the nozzle center line.

Nozzle thrust ratio characteristics for wedge angles of 0°, 12°, and 24° are shown to the right of Fig. 9. The dashed lines representing no turning loss for each of the respective wedge deflections is simply

$$\left(\frac{F_j}{F_i}\right)_{\text{no loss}}=\cos \delta_{\text{static}}\left(\frac{F_j}{F_i}\right)_{\delta_w=0°} \tag{3}$$

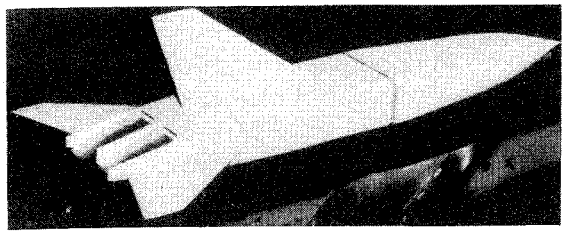

Fig. 7 Overall view of model with two-dimensional wedge nozzles.

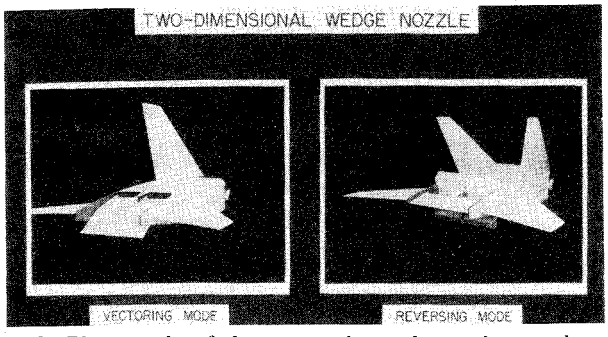

Fig. 8 Photographs of thrust vectoring and reversing nozzle configurations.

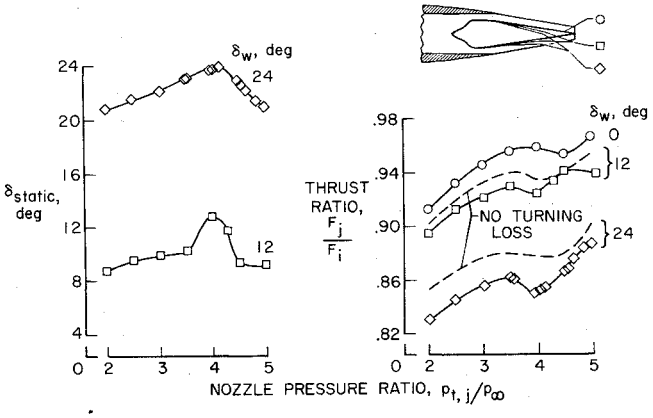

Fig. 9 Static performance of two-dimensional wedge nozzle.

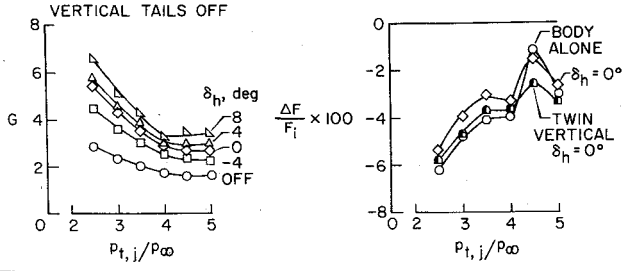

Fig. 10 Effect of model geometry on gain factor and thrust recovery, $\delta_W = 12°$, $M = 0.60$, $\alpha = 0°$.

Static turning losses of about 1% for the 12° wedge and 2% for the 24° wedge occur. As will be subsequently seen, the static turning losses affect performance at forward speeds and indicate an area of research that is needed to optimize wedge geometry in order to minimize these losses.

Lift augmentation characteristics for the nozzle with the 12° wedge at $M = 0.6$ are shown in Fig. 10 for the body alone, and with horizontal tail deflections varying from −4° to 8°. The increases in gain factor noted for the addition of horizontal tails are due to increases in jet-induced supercirculation lift since the jet lift is the same for all cases. Somewhat higher gains would be expected for this nozzle than for the vectored thrust model previously discussed because of partial-span ef-

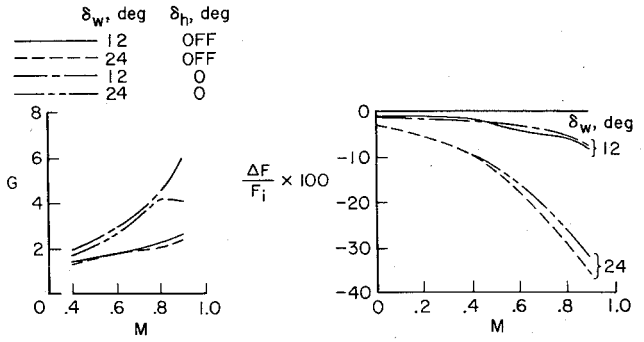

Fig. 11 Effect of Mach number on gain factor and thrust recovery, $p_{t,j}/p_\infty = 4.0$, vertical tails off.

fects. The two-dimensional nozzle ratio of nozzle width to horizontal-tail span is some 18% higher than the vectored thrust model. In addition, by virtue of the jet flow over and under the wedge, the nozzle more closely resembles a blown flap (blowing over and under a wing trailing-edge flap) which produces more induced lift than a pure jet flap, because the wedge contributed some aerodynamic lift.

The effect on gain factor, of adding the single or twin vertical tails with the horizontal tail at $\delta_h = 0°$, is small (not shown). The largest effect is for the 12° wedge at $M = 0.9$ where an 8% to 10% loss in gain factor occurred at both tail deflections of 0° and 4°. For the 24° wedge, (not shown) there was no effect of adding the twin vertical tails and gain factors are approximately the same as for the 12° wedge up to $M = 0.6$. Note that the same gain factor for the 24° wedge would have approximately twice the value of incremental lift as a result of increases in both jet and induced lift.

Thrust recovery for this nozzle is defined similar to Ref. 8 and is in terms of ideal thrust

$$\frac{\Delta F}{F_i} = \left(\frac{F-D}{F_i}\right)_{\delta_w} - \cos\delta_{\text{static}}\left(\frac{F-D}{F_i}\right)_{\delta_w=0°} \tag{4}$$

Typical recovery characteristics in percent ideal thrust are shown in Fig. 10 at $\delta_w = 12°$ and $M = 0.6$, and illustrate the major effects of external geometry changes on recovery. First, note that losses for the nozzle alone (tails off) range from about 6% at low-pressure ratio to about 1% at $p_{t,j}/p_\infty = 4.5$ which is the pressure ratio at which the static thrust ratio indicated the least loss due to turning (Fig. 9). Thus, it would seem reasonable to assume that with proper design, these losses could be minimized or eliminated.

Adding the horizontal tails at $\delta_h = 0°$, resulted in a small increase (less negative) in recovery. This increase in recovery is probably due to a decrease in drag on the tails that results from the induced upwash field created by the vectored jet exhaust (Fig. 10). However, the net change in recovery due to adding horizontal tails is also a function of tail deflection as an additional 4% loss (added to tails-off value) occurs for $\delta_h = 8°$ at $p_{t,j}/p_\infty = 4.5$. The twin vertical tails cause a reduction in recovery due to unfavorable interference effects.[15] This interference is caused by misalignment of the vertical tails with the local body flowfield. It should be noted that the tail location was fixed to a single position.

Figure 11 presents the effects of Mach number on both gain factor and thrust recovery at a nozzle pressure ratio of 4.0 (design pressure ratio). There is an increase in gain factor with Mach number for both the 12° and 24° wedges except as noted. The effect of varying wedge angle from 12° to 24° is also small except at $M = 0.9$ for $\delta_h = 0°$. The loss in gain factor for the 24° wedge between $M = 0.8$ and 0.9 may be a result of premature separation on the plug resulting from adverse interference of the horizontal tails. The increase in gain factor of adding the horizontal tails for either wedge angle is simply due to the additional lift induced on the tails.

Thrust recovery characteristics are shown to the right of Fig. 11. As Mach number is increased, losses due to vectoring increase for the nozzle with both wedge angles. It would appear from the recovery characteristics that this nozzle in the vectoring mode could be used for in-flight thrust reversing. This, of course, is highly dependent upon not only the aircraft, but also particular flight requirements.

Upper Surface Blowing

An exploratory study to determine the feasibility of utilizing upper surface blowing for lift augmentation on fighter aircraft at transonic speeds has been the subject of a recent joint USAF/Boeing/NASA investigation. This model, shown in Fig. 12, had a rectangular nozzle exit with an internal deflection angle of 15° that exhausted over a Coanda flap located at the center of the wing trailing edge. The wing also had full-span leading-edge flaps outboard of the wing strake and trailing-edge flaps extending outboard from the center flap to 88% of the wing semispan. This model used the same nonmetric forebody and internal propulsion-simulation system with the single thrust-drag balance as that of Ref. 10. The wing panels outboard of the strake were identical to those used in an investigation of high-lift devices on a fighter airplane model.[16]

The nozzle static turning characteristics are also shown in Fig. 12. Included for reference is the turning angle for the nozzle alone (all wing and flap area removed downstream of nozzle exit) which shows that the maximum measured δ_{static} was about 5° less than the design turning angle of 15°. This decrease may be associated with flow separation over the nozzle lower surface. Addition of the wing and Coanda flap affect turning by what appears to be both reattachment and separation of the flow ($\delta_F = 0°$ and 5°) and just separation over the flap ($\delta_F = 10°$ and 15°). Note that as flap angle is increased from 5° to 15°, the pressure ratio at which separation occurs decreases. Static tests were also made with the wing trailing-edge angle the same as the Coanda flap angle, and these tests showed no effect of the trailing-edge flap on turning angle, thus indicating no apparent spreading of the jet laterally at static conditions.

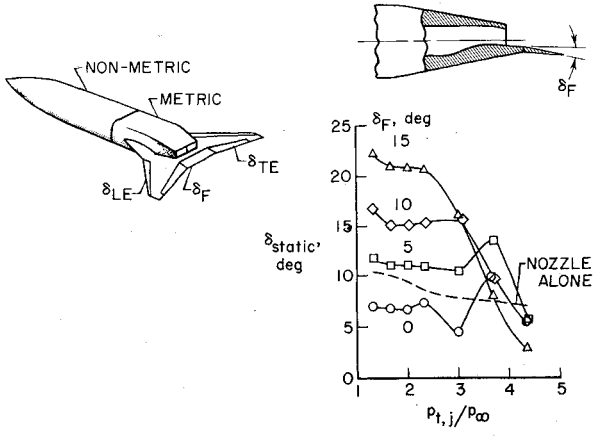

Fig. 12 Static turning performance of upper surface blowing configuration.

Lift characteristics of this propulsive-lift system at $M = 0.7$ are presented in Fig. 13. Incremental lift at $\delta_F = 0°$ and $\delta_{LE} = \delta_{TE} = 0°$, shown to the upper left, reflect the effect of the flow separation on the Coanda flap previously shown in the static data of Fig. 12. The maximum value of incremental lift occurs at or near the pressure ratio at which the separation is occurring. Approximately half the maximum incremental lift shown for $\delta_F > 0°$ was induced lift.

An indication of the effectiveness of the trailing and leading-edge flaps in conjunction with the Coanda flap is illustrated to the upper right of Fig. 13. Incremental lift is shown as a function of nozzle pressure ratio for various combinations of δ_F, δ_{TE}, and δ_{LE} equal to 10°. Ten deg deflection of the wing trailing-edge flaps produced a small increase in ΔC_L, indicating some lateral spreading of the jet. This was observed only for $\delta_{TE} = 10°$ or 15° with the Coanda flap and the trailing-edge flap deflections equal. There was little or no effect of the leading-edge flap at this angle of attack (same result at $\delta_F = 0°$). The effect of angle of attack at $p_{t,j}/p_\infty = 3.0$ with $\delta_{LE} = \delta_{TE} = 0°$ is shown in the lower portion of Fig. 13. In general, incremental lift increases as angle of attack increases. Note that the incremental values of lift due to power would be added to the jet-off lift of a particular configuration, the value of which is dependent upon flap deflection angles.

The effects of upper surface blowing on the drag of the configuration with the Coanda flap at 10° can be seen by examining the drag polars shown at $M = 0.7$ in Fig. 14. Two

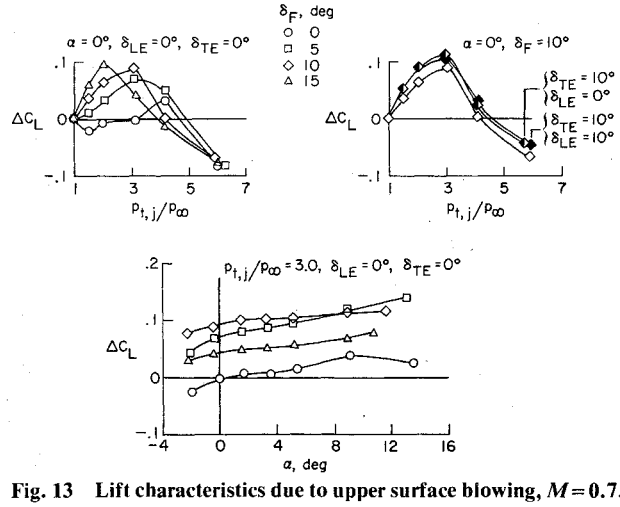

Fig. 13 Lift characteristics due to upper surface blowing, $M = 0.7$.

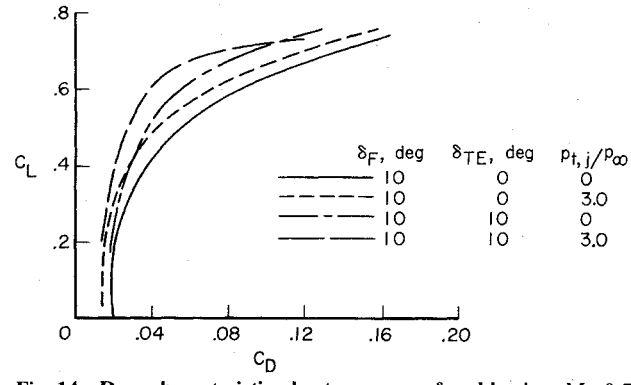

Fig. 14 Drag characteristics due to upper surface blowing, $M = 0.7$.

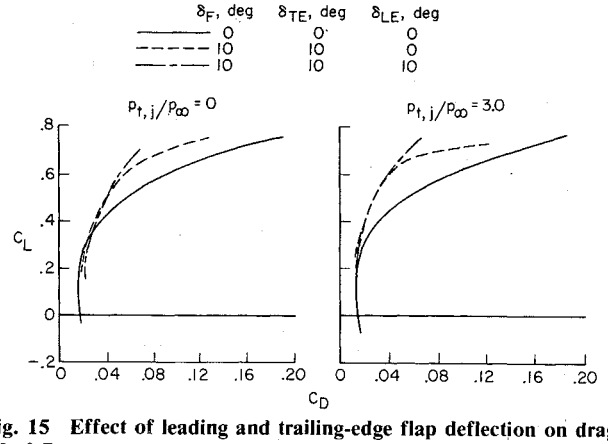

Fig. 15 Effect of leading and trailing-edge flap deflection on drag, $M = 0.7$.

effects are illustrated. first, deflecting the wing trailing-edge flaps from 0° to 10°, jet-off, show the typical improvement in drag expected from increasing wing camber. Power effects result in further decreases in drag that are probably due to the wing operating in an induced upwash field similar to that previously described for the vectored thrust model. Some improvements in span loading would also be anticipated. The magnitude of the power effects are, of course, dependent on pressure ratio.

The overall improvement of the drag polars resulting from deflection of the leading and trailing-edge flaps and Coanda flap combined with power effects are shown in Fig. 15 at $M = 0.70$ and at nozzle pressure ratios of 0 and 3.0. For example, the jet-off data show that for maximum performance at high lift coefficients, the leading-edge flap would be deployed at a high lift coefficient of about 0.5. The effect of power shown to the right of Fig. 15 is to shift the drag polars up, resulting in a decrease in drag at constant lift coefficient.

Conclusions

Supercirculation effects induced from thrust vectoring generally resulted in increases in lift and decreases in drag at constant angle of attack. There also was an increase in maximum usable lift coefficient due to thrust vectoring. However, although thrust vectoring with a practical nozzle configuration such as a two-dimensional wedge nozzle did induce lift, significant turning losses occurred. Drag reduction at high lift coefficients was also found for a concept utilizing upper surface blowing. These studies have, for the most part, been conceptual. Additional research is required of complete aircraft configurations employing these powered-lift concepts in order to ascertain the extent of performance gains.

References

[1]Runckel, J. F., Schmeer, J. W., and Cassetti, M. D., "Performance, Stability and Control Investigation at Mach Numbers from 0.4 to 0.9 of a Model of the 'Swallow' With Outer Wing Panels Swept 25°; With and Without Power Simulation," NASA TM SX-296, 1960.

[2]Schmeer, J. W. and Cassetti, M. D., "Performance, Stability and Control at Mach Numbers From 0.6 to 1.05 of a Model of the 'Swallow' With Outer Panels Swept 75° With and Without Power Simulation," NASA, TM SX-306, 1960.

[3]Schmeer, J. W., Cassetti, M. D., and Simonson, A. J., "Transonic Aerodynamic Characteristics of a Model of a Single-Engine Four-Jet V/STOL Airplane," NASA, TM SX-528, 1961.

[4]Schmeer, J. W. and Runckel, J. F., "Jet Interference Effects on a Model of a Single-Engine Four-Jet V/STOL Airplane at Mach Numbers From 0.60 to 1.00," NASA, SX-685, 1962.

[5]Salters, L. B., Jr. and Schmeer, J. W., "Longitudinal Aerodynamic and Propulsion Characteristics of a Propulsion-Wing V/STOL Model at High Subsonic Speeds," NASA, TM X-2693, 1973.

[6]Maiden, D. L. and Mercer, C. E., "Performance Characteristics of a Single-Engine Fighter Model Fitted With an In-Flight Thrust Reverser," NASA, TN D-6460, 1971.

[7]Mercer, C. E., and Maiden, D. L., "Effects of an In-Flight Thrust Reverser on the Stability and Control Characteristics of a Single-Engine Fighter Airplane Model," NASA, TN D-6886, 1973.

[8]Corson, B. W., Jr., Capone, F. J., and Putnam, L. E., "Lift Induced on a Swept Wing by a Two-Dimensional Partial-Span Deflected Jet at Mach Numbers From 0.20 to 1.30," NASA, TM X-2309, 1971.

[9]Capone, F. J., "Exploratory Investigation of Lift Induced On a Swept Wing By a Two-Dimensional Partial-Span Deflected Jet at Mach Numbers From 0.20 to 1.30," NASA, TM X-2529, 1972.

[10]Capone, F. J., "The Effects of Vectoring a Partial-Span Rectangular Jet on Propulsion-Induced Aerodynamic Forces at Mach Numbers From 0.40 to 1.20," NASA, TN D-8039, 1975.

[11]Capone, F. J., "Effects of Nozzle Location and Shape on Propulsion-Induced Aerodynamic Characteristics Due to Vectoring Twin Nozzles at Mach Numbers From 0.40 to 1.20," NASA, TM X-3313, 1975.

[12]Capone, F. J., "Supercirculation Effects Induced by Vectoring a Partial-Span Rectangular Jet," *Journal of Aircraft*, Vol. 12, Aug. 1975, pp. 633-638.

[13]Runckel, J. F., "Interference Between Exhaust System and Afterbody of Twin-Engine Fuselage Configurations," NASA, TN D-7525, 1974.

[14]Maiden, D. L., "Performance of an Isolated Two-Dimensional Variable-Geometry Wedge Nozzle With Translating Shroud and Collapsing Wedge at Speeds Up to Mach Number 2.01," NASA TN D-7906, 1975.

[15]Maiden, D. L. and Petit, J. E., "Investigation of Two-Dimensional Wedge Nozzles for Advanced Aircraft," *Journal of Aircraft*, this issue, pp. 809-816.

[16]Capone, F. J., "Effect of Various Wing High-Lift Devices on the Longitudinal Aerodynamic Characteristics of a Swept-Wing Fighter Model at Transonic Speeds," NASA, TM X-3204, 1975.